

In Situ Constructed Magnetic Core-Shell Hydrogen-Bonded Organic Framework-on-Metal-Organic Framework Structure: an Efficient Catalyst for Peroxymonosulfate **Activation**

Yingying Du, Chenhui Ding, Chao Deng, Susanta Banerjee, and Seema Agarwal*

Zeolite imidazole-based framework (ZIF-67), a notable class of metal-organic frameworks (MOFs), shows promise in activating peroxymonosulfate (PMS) for pollutant degradation due to its uniformly distributed cobalt ions. However, its nanoparticle form and the elution of cobalt ions during use cause challenges in recycling and the risk of secondary pollution. In this study, a magnetic core-shell hydrogen-bonded organic framework (HOF) on the MOF (HOF-on-Fe₃O₄/ZIF-67) is successfully prepared. The porous HOF shell not only protects the active sites and mitigates cobalt ion leaching but also reduces mass transfer limitations, ensuring sustained catalytic performance. The magnetic Fe₃O₄ core enhances electron transfer between cobalt ions, boosts catalytic efficiency, and facilitates easy separation and recycling. This core-shell structure effectively activates PMS, achieving 100% removal of Rhodamine B, a model wastewater dye, within 10 min (Rh B = 50 mg L^{-1} , HFZ = 150 mg L^{-1} , PMS = 1.5 mm, pH = 7, room temperature). Furthermore, under the protection of the HOF shell, cobalt ion leaching is minimized to a negligible value (0.14 mg L⁻¹) after 5 cycles of use. The research provides fresh perspectives into the development of core-shell composite materials with improved performance and recyclability in wastewater treatment.

1. Introduction

The sulfate radical-advanced oxidation process (SR-AOP) is highly effective at decomposing toxic and persistent organic

Y. Du, C. Ding, C. Deng, S. Agarwal Advanced Sustainable Polymers Macromolecular Chemistry 2 and Bavarian Polymer Institute University of Bayreuth Universitätsstrasse 30, 95440 Bayreuth, Germany

E-mail: agarwal@uni-bayreuth.de

S. Banerjee

Materials Science Centre Indian Institute of Technology Kharagpur Kharagpur 721302, India



The ORCID identification number(s) for the author(s) of this article can be found under https://doi.org/10.1002/adfm.202416686

© 2024 The Author(s). Advanced Functional Materials published by Wiley-VCH GmbH. This is an open access article under the terms of the Creative Commons Attribution License, which permits use, distribution and reproduction in any medium, provided the original work is properly

DOI: 10.1002/adfm.202416686

contaminants, positioning it as a leading technology for wastewater treatment.[1] Sulfate radicals (SO4*-) commonly formed by the activation of persulfate (PS, S2O82-) or peroxymonosulfate (PMS, HSO₅-) exhibit a high redox potential (2.5-3.1 V), a wider pH range (3-9), longer stability, and superior reaction selectivity.[2,3] PMS, with its asymmetric structure, is more easily activated than PS and is environmentally friendly, which makes it widely used in industry.^[4] Transition metal ions (Cu²⁺, Ni^{2+} , Fe^{2+} , Co^{2+} , and Mn^{2+}), metal oxides (Co₃O₄, Fe₃O₄, Mn₃O₄) ultrasound, ultraviolet irradiation, and electrochemistry methods are employed to activate PMS.[5] Among them, cobalt-based catalysts (especially Co²⁺) are thermodynamically more favorable for combining with HSO₅⁻ having lower Gibbs free energy values, and are considered the most ideal PMS activators.[6] The zeolite-like imidazole frame-

work (ZIF-67), an important category of metal-organic frameworks (MOFs), is constructed with cobalt serving as the metal component and 2-methylimidazole (2-MeIM) as the organic ligand. This framework features an abundance of divalent cobalt species uniformly dispersed throughout, high porosity, and excellent chemical stability, attributes that have attracted considerable scholarly attention.^[7] Studies have demonstrated that PMS can be effectively activated by ZIF catalysts to degrade organic pollutants, highlighting their potential as promising cobalt-based catalysts.^[8] However, the practical application of ZIF-67 in PMS activation is impeded by its nanoparticle form, which complicates recyclability. Additionally, the leaching of cobalt ions during use raises concerns about secondary pollution and poses risks to both the ecosystem and human health.^[9] Therefore, it is imperative to design catalysts that enhance both service life and stability to address these

To overcome these challenges, the development of core-shell composite materials has proven to be highly effective. For instance, Wu et al. created a Fe₃O₄@Zn/Co-ZIFs core-shell structure and achieved quantitative removal of carbamazepine in a short time.^[10] Similarly, Wan et al. synthesized a core-hetero shell magnetic composite material, ZIF-67/vanadium titanium www.advancedsciencenews.com



www.afm-journal.de

magnetite, which effectively activated PMS and achieved a 93.3% removal rate of levofloxacin within 60 min.^[11]

However, in traditional core-shell structures, the shell usually does not participate in the reaction and primarily serves a protective role. This limits the full potential of the core-shell structure. Furthermore, the shell coating can hinder the exposure of active sites, leading to reduced catalytic performance. Consequently, selecting appropriate shell materials is crucial to enhance both the protective function and the catalytic activity.

Hydrogen-bonded organic frameworks (HOFs) are recognized as a promising group of crystalline materials, attracting widespread attention from scholars due to their well-defined structures and multifunctional properties. [12] Notably, HOF-102 demonstrates excellent stability and chemical resistance, with its porosity facilitating the enrichment of dyes. [13] This characteristic enables dye aggregation on the catalyst surface, effectively shortening the degradation path and accelerating the breakdown of organic pollutants. Consequently, HOF is considered an excellent choice for shell materials. However, to our knowledge, there are currently no literature reports evaluating HOF-on-MOF materials in SR-AOP.

In this study, we developed a magnetic HOF-on-MOF-type core-shell catalyst (HOF-on-Fe₃O₄/ZIF-67, referred to as HFZ) using ZIF-67 as the core incorporated with magnetic Fe₃O₄. The inclusion of Fe₃O₄ enhances electron transfer between cobalt ions, thereby improving catalytic performance and facilitating the quick and easy separation and recovery of the catalyst after use. The porous HOF shell minimizes mass transfer limitations and protects the active sites, effectively reducing the leaching of cobalt ions during use while maintaining strong catalytic performance. This unique core-shell structure makes it an ideal catalyst for PMS activation. The catalyst efficiently activated PMS, achieving 100% removal of a model dye (Rhodamine B, Rh B) within 10 min, and demonstrated effective degradation across a wide pH range (3–9) with minimal cobalt ions leaching (0.14 mg L^{-1} after 5 cycles). This research strategy not only broadens the application of HOF materials in water treatment but also provides new insights into the preparation of core-shell composite materials for use in SR-AOP.

2. Results and Discussion

The preparation strategy for the HFZ is illustrated in **Figure 1a**. Initially, Fe₃O₄ nanoparticles were introduced into the reaction solution having precursors of ZIF-67 to achieve in situ growth of Fe₃O₄/ZIF-67 particles. Next, these Fe₃O₄/ZIF-67 particles were dispersed in an acetone solution, to which a dimethylformamide (DMF) solution of the HOF precursor was added dropwise and stirred overnight. Finally, the products (HFZ particles) were collected using an external magnet. The morphology and particle size of the materials were analyzed by scanning electron microscopy (SEM) and transmission electron microscopy (TEM). Fe₃O₄ nanoparticles maintain a consistent spherical shape with a particle size of 23.8 \pm 1.92 nm (Figure 1b). ZIF-67 particles had a size of \approx 823 \pm 75 nm and were rhombohedral dodecahedron in structure (Figure 1c).[14] The average diameter of Fe₃O₄ nanoparticles and ZIF-67 was calculated with ImageI software by randomly selecting 50 particles in SEM images. HOF showed a rod-like structure (Figure S1, Supporting Information), and the structure of HOF is shown in Figure S2 (Supporting Information). The overall morphology of the synthesized Fe₃O₄/ZIF-67 (Figure 1d) maintains the rhombohedral dodecahedron shape. with numerous Fe₃O₄ nanoparticles distributed on the surface and within the bulk of the ZIF-67 particles. The TEM image of Fe₃O₄/ZIF-67 (Figure 1f) confirms the presence of Fe₃O₄ within the ZIF-67 core. The surface of the HFZ particles is distinctly covered by the HOF coating while preserving the rhombohedral dodecahedron shape (Figure 1e). TEM images of HFZ (Figure 1g) reveal two distinct regions: a darker core, representing the Fe₃O₄/ZIF-67, surrounded by lighter regions indicating the HOF coating. The enlarged TEM image (Figure 1h) clearly shows an interfacial layer of rough HOF shell (thickness ≈44 nm) around the Fe₃O₄/ZIF-67 core. Overall, the magnetic HFZ coreshell structure is confirmed by SEM and TEM. Additionally, x-ray energy dispersive spectroscopy (EDS) elemental mapping of individual HFZ particles demonstrates the presence of C, N, O, Fe, and Co elements in the core-shell particles (Figure 1i).

The x-ray diffraction (XRD) patterns of Fe_3O_4 , HOF, ZIF-67, and HFZ are shown in **Figure 2a**. In the XRD pattern of HFZ, 2 theta corresponds to the (100) crystal plane at 3.6°, which belongs to the characteristic diffraction peak of HOF. ^[15] 7.4°, 10.5°, 12.9°, 14.8°, 16.6°, and 18.2° correspond to the (011), (002), (112), (022), (013) and (222) crystal planes, which are highly consistent with the ZIF-67 crystal. ^[16] And 30.5°, 35.6°, 43.6°, 57.5°, and 62.8° are attributed to (220), (311), (400), (511) and (440) crystal planes, which are highly matched with the characteristic diffraction peaks of Fe_3O_4 nanoparticles. ^[17] These results confirmed the successful preparation of HFZ without affecting significantly the crystal structure of ZIF-67.

The structural analysis by Fourier transform infrared spectroscopy (FT-IR) (Figure 2b) confirmed expected peaks at 625 cm⁻¹ (Fe—O bond), and 574 cm⁻¹ (Fe₃O₄), aligning well with the literature.^[18] The peak at 425 cm⁻¹ is attributed to the stretching vibration of Co—N in the ZIF-67 crystal, while the peaks at 1418 and 1580 cm⁻¹ correspond to the stretching modes of the C—N bond in imidazole.^[19] These characteristic peaks observed in the FT-IR spectra of HFZ confirm the successful synthesis of HFZ.

The electrochemical impedance spectroscopic (EIS) analysis of HFZ and HOF-on-ZIF-67 revealed that the Nyquist plot for HFZ shows a smaller semicircle compared to HOF-on-ZIF-67 (Figure 2c). This suggests that HFZ exhibits a relatively lower charge transfer resistance, which is due to the enhanced charge transfer facilitated by the incorporation of Fe₃O₄.^[20] The Tafel polarization curve analysis further supports this observation (Figure 2d). The free corrosion potentials for HFZ and HOF-on-ZIF-67 are -0.27 and -0.18 V. This suggests a faster electron transfer rate for HFZ compared to HOF-on-ZIF-67. The findings show that incorporating Fe₃O₄ significantly improves the electron transfer ability of HFZ, contributing to the rapid and efficient degradation of organic pollutants. Additionally, a vibrating sample magnetometer (VSM) was employed to assess the magnetic properties (Figure 2e). The saturation magnetization (Ms) values for Fe₃O₄ nanoparticles and HFZ were 50.3 and 27.6 emu g⁻¹, respectively. The decrease in magnetic strength for HFZ is primarily due to the ZIF-67 and HOF coatings. Nonetheless, the strong magnetic response of HFZ allows for easy separation using an external

doi/10.1002/adfm.202416686 by Universitaet Bayreuth, Wiley Online Library on [11/11/2025]. See the Terms and Conditions (https:

and-conditions) on Wiley Online Library for rules of use; OA articles are governed by the applicable Creative Commons

www.afm-journal.de

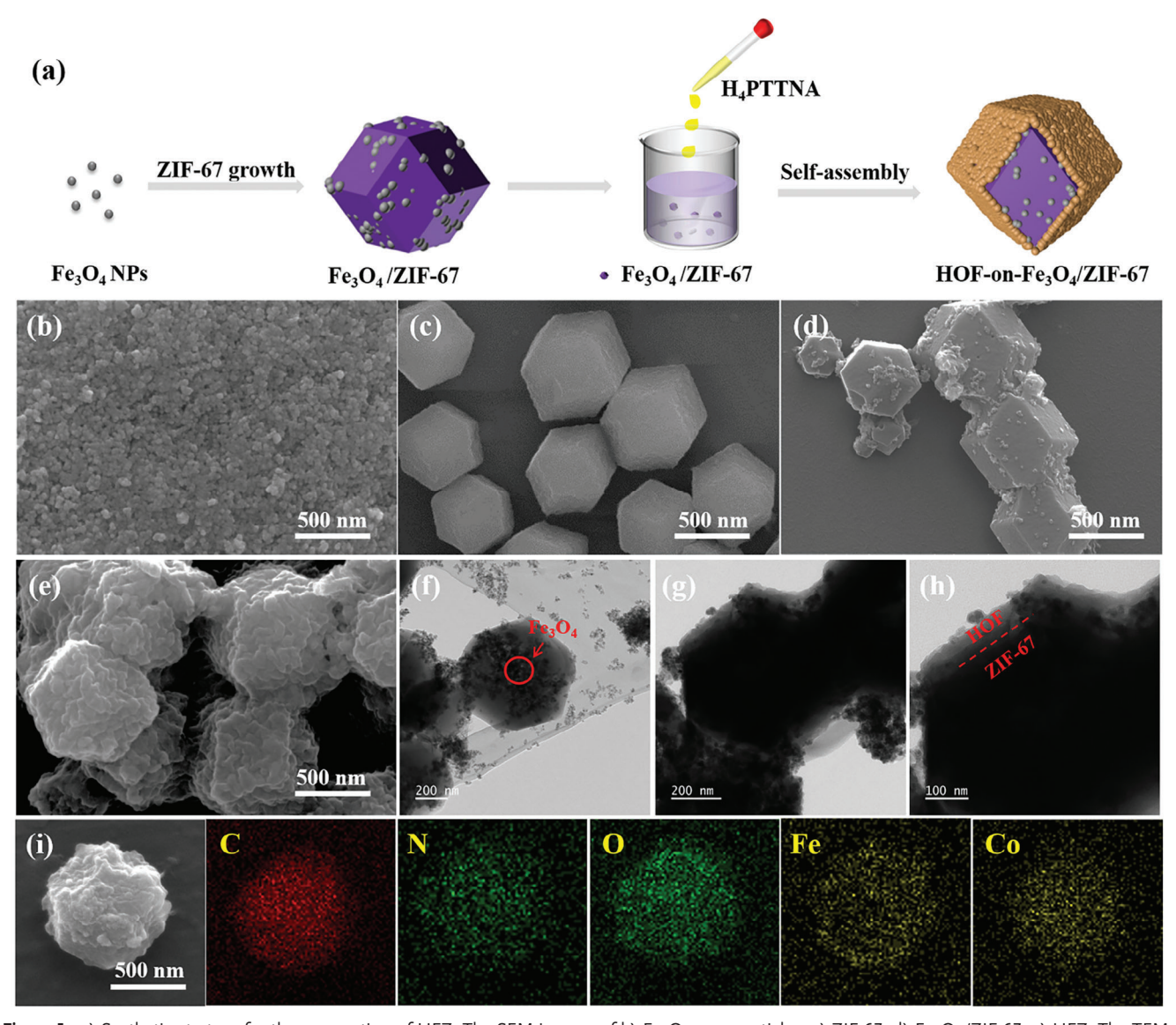


Figure 1. a) Synthetic strategy for the preparation of HFZ. The SEM images of b) Fe_3O_4 nanoparticles, c) ZIF-67, d) Fe_3O_4 /ZIF-67, e) HFZ. The TEM images of f) Fe_3O_4 /ZIF-67, g) and h) HFZ. i) EDS elemental mapping images of HFZ.

magnet, facilitating the collection, recycling, and reuse of the catalyst.

As a refractory organic pollutant, Rh B released into water can cause cancer in humans, pollute water and soil, and harm the ecosystem. Therefore, in our study, Rh B was selected as a model organic contaminant to assess the performance of HFZ in activating PMS as a catalyst. Before the actual experiment of evaluating catalytic performance, the dye enrichment effect of the individual components of the core-shell structure was conducted (Figure S3, Supporting Information). It was observed that the adsorption capacities of Fe $_3$ O $_4$ nanoparticles and ZIF-67 for Rh B were relatively low, with maximum values of 1.5 and 14.3 mg g $^{-1}$, respectively. This low adsorption is likely due to the large molecular structure of Rh B, resulting in minimal interaction with the surfaces of these materials. In contrast, HOF exhibited a high adsorption capacity for Rh B, reaching 265.3 mg g $^{-1}$. This high

capacity can be attributed to the high porosity and porous structure in addition to the electrostatic interaction between cationically charged dye and HOF.[15] These results suggest that the HOF shell in the composite material effectively enriches the dye, concentrating Rh B which might be promising for dye degradation. The effectiveness of different systems in removing Rh B was then analyzed, and the results are shown in Figure 3a and Figure S4 (Supporting Information). Fe₃O₄ and ZIF-67 alone exhibited negligible removal efficiencies (1.6% and 3.1%, respectively). The HFZ system, however, achieved a 12.6% reduction in Rh B within 20 min. This reduction may be attributed to the HOF shell of HFZ adsorbing Rh B, as HOF alone also showed considerable adsorption of Rh B. The Rh B removal rate with PMS alone was just 8.6%, suggesting that PMS by itself cannot be effectively activated to generate free radicals. In the Fe₃O₄ and PMS system, 14.2% of Rh B was removed, indicating that Fe₃O₄ by itself is not

16163028, 0, Downloaded from https://advanced.onlinelibrary.wiley.com/doi/10.1002/adfm.202416686 by Universitaet Bayreuth, Wiley Online Library on [11/11/2025]. See the Terms

ms) on Wiley Online Library for rules of use; OA articles are governed by the applicable Creative Commons License

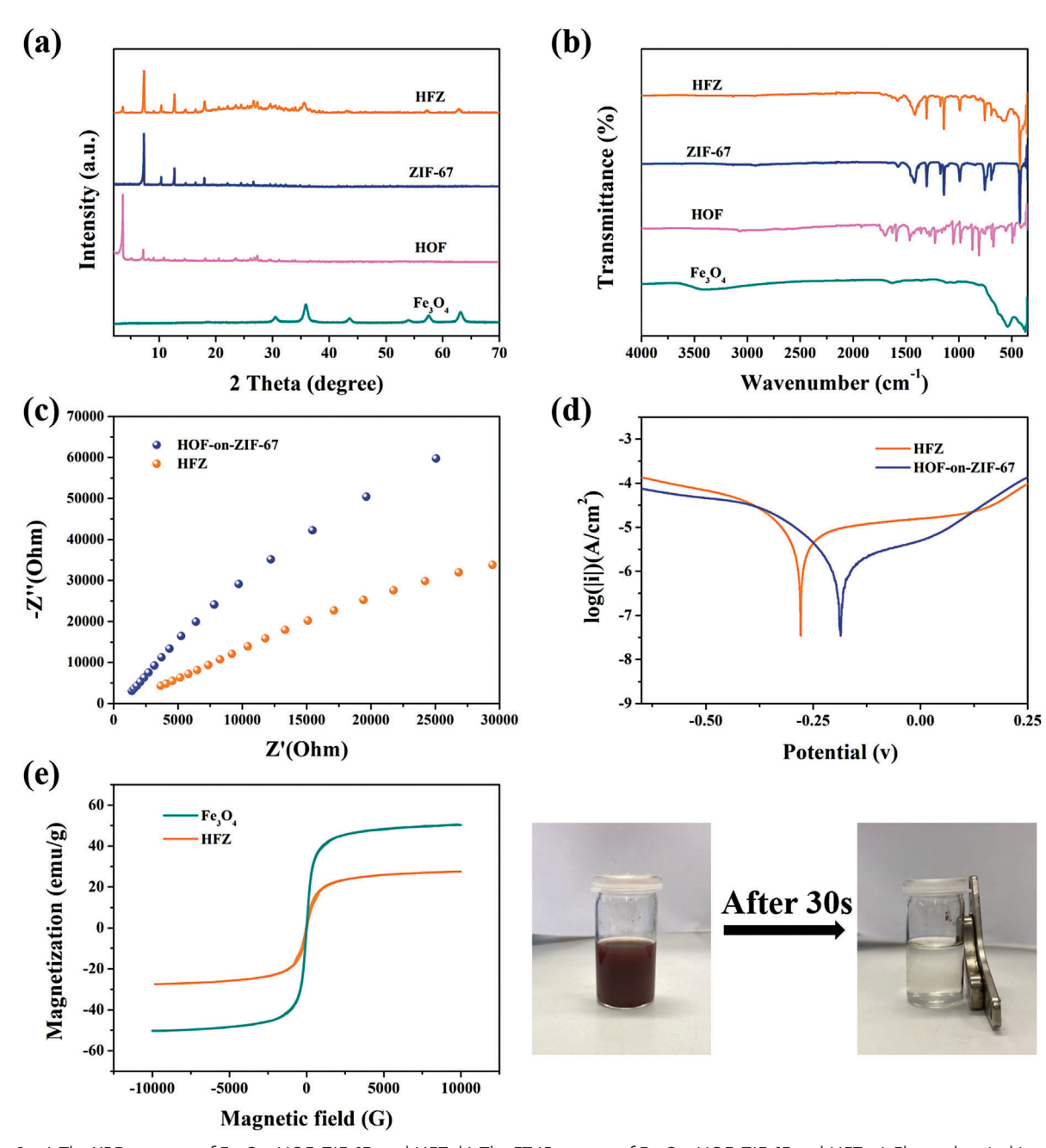


Figure 2. a) The XRD patterns of Fe_3O_4 , HOF, ZIF-67, and HFZ. b) The FT-IR spectra of Fe_3O_4 , HOF, ZIF-67 and HFZ. c) Electrochemical impedance spectroscopic (EIS) analysis and d) Tafel polarization curves of HFZ and HOF-on-ZIF-67. e) Magnetic hysteresis loops of Fe_3O_4 and HFZ. And HFZ has excellent magnetic separation using an external magnet (30 s).

highly effective in activating PMS. The HFZ together with PMS removed 72.4% of Rh B within 1 min, with the removal efficiency reaching up to 97.5% after 3 min of reaction and nearly complete removal within 10 min. This demonstrates that HFZ plays a crucial role in activating PMS, leading to the rapid removal of Rh B. Initially, as shown in Figure 3a, the dye degradation efficiency of ZIF-67 activated PMS appears almost the same as that of HFZ. As the total amounts (mass) of HFZ and ZIF-67 used in the experiments were the same, the actual amount of activating ZIF-67 in HFZ is less than that in pure ZIF-67. This actually indi-

cates that HFZ-activated PMS is more efficient, as it contains less ZIF-67 compared to pure ZIF-67. This demonstrates that introducing ${\rm Fe_3O_4}$ can enhance electron transfer between cobalt ions and accelerate the degradation rate of organic matter. We compared the efficiency of HFZ with some literature known related systems (Figure 3b) and demonstrated a new, efficient dye degradation system. The values for CuS-PVP@ZIF-67, MnFe₂O₄/ZIF-67, CuFe₂O₄@ZIF-67, Fe₃O₄-PVP@ZIF-67, NF/ZIF-67, and cal-ZIF-67/Ac in Figure 3b were taken from literatures cited as in the reference section. [21]

ons) on Wiley Online Library for rules of use; OA articles are governed by the applicable Creative Commons

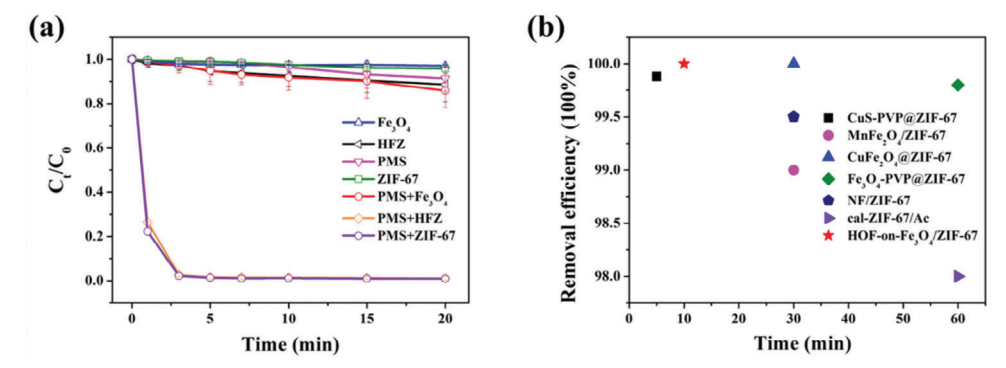


Figure 3. a) The removal of Rh B using different systems, reaction condition: Rh B; 50 mg L^{-1} , 100 mL, 1.5 mm PMS, rt., pH = 7. b) Comparison of HFZ/PMS system with other reported MOF-based and/or metal oxide catalysts in Rh B removal.

To further explore the performance of HFZ, we analyzed the effects of Rh B concentration, PMS contents, HFZ dosages, and solution conditions on degradation efficiency. **Figure 4a** shows the effect of a constant amount of HFZ in degrading different initial concentrations of Rh B (25 to 150 mg L $^{-1}$) keeping the PMS concentration and the pH constant. As the concentration of Rh B increased from 25 to 150 mg L $^{-1}$, the removal efficiency dropped significantly from 97% to 6% within 1 min, accompanied by a decrease in the rate constant of degradation k from 3.35 to 0.064 min $^{-1}$ (Figure S5, Supporting Information). The removal of Rh B in higher concentrations (150 mg L $^{-1}$) took longer and reached \approx 64% degradation in 10 min. After this time, the rate of dye reduction decreased from 3.2 to 0.1 mg min $^{-1}$, resulting in a total reduction of 74% after 20 min. At Rh B concentrations up to 50 mg L $^{-1}$, full removal occurred within 10 min. Figure 4b

illustrates how varying PMS dosages influence the degradation of Rh B, using a constant concentration of 50 mg L $^{-1}$ and a fixed amount of HFZ. With a PMS dosage of 0.5 mm, 27% of Rh B was eliminated in 1 min, and the efficiency increased to 77.3% after 20 min, indicating that the catalytic performance was unsatisfactory with insufficient PMS concentration. As the PMS dosage rose from 0.5 to 1.5 mm, the catalytic performance was significantly enhanced, and the degradation rate constant k shifted from 0.197 to 0.825 min $^{-1}$ (Figure S6, Supporting Information). At a PMS dosage of 1.5 mm, Rh B is almost completely removed within 10 min. However, raising the PMS dosage to 2.5 mm resulted in only a slight improvement in Rh B removal, with the k value reaching 0.876 min $^{-1}$. Therefore, considering both economic and practical factors, 1.5 mm PMS is selected as the optimal dosage for catalytic degradation.

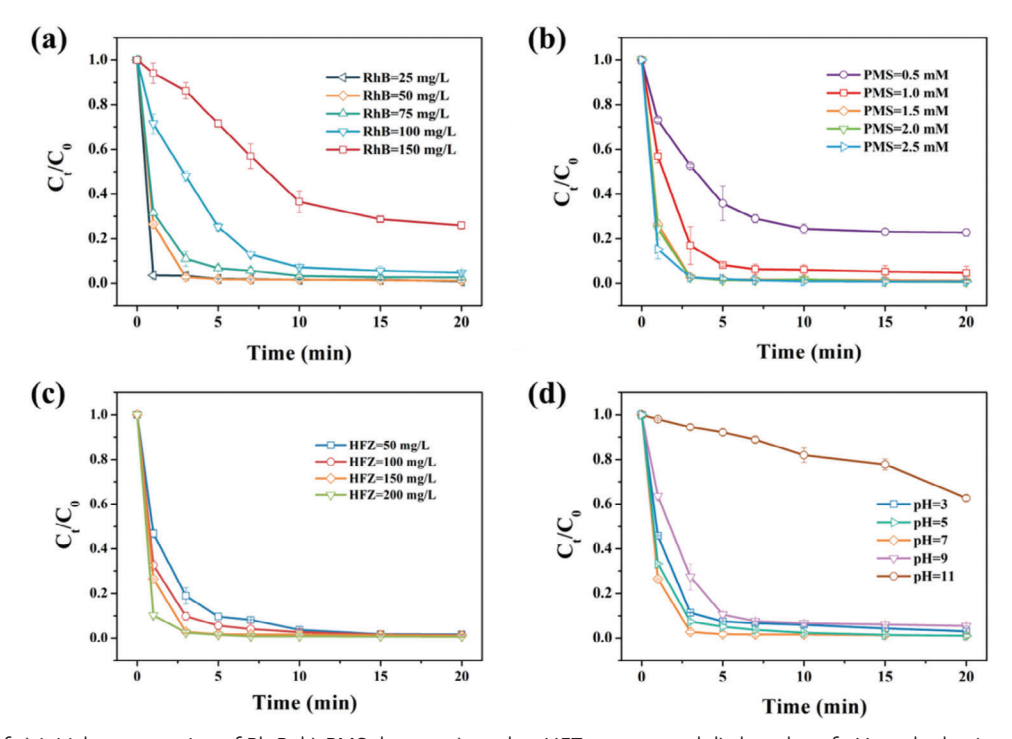


Figure 4. Effect of a) initial concentration of Rh B, b) PMS dosage, c) catalyst HFZ content, and d) the value of pH on rhodamine removal efficiency. Reaction condition: 100 mL Rh B = 50 mg L^{-1} , PMS = 1.5 mm, HFZ = 150 mg L^{-1} , pH = 7, rt.

www.afm-journal.de

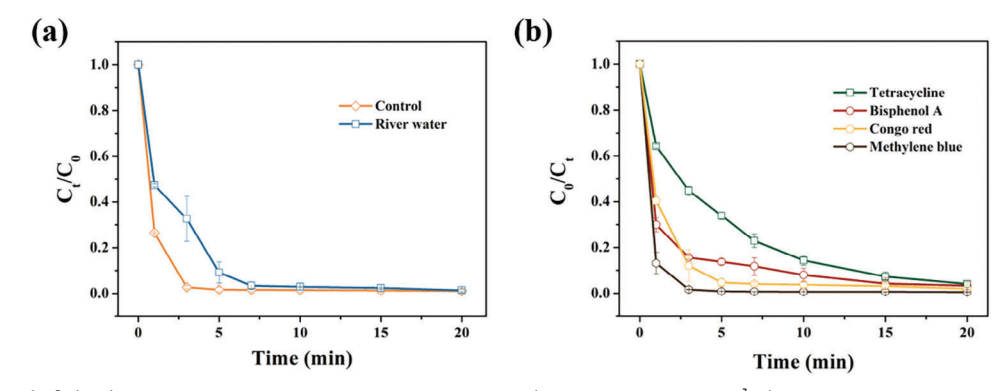


Figure 5. a) Removal of Rh B by HFZ/PMS system in river water, reaction condition: $100 \text{ mL} 50 \text{ mg L}^{-1} \text{ Rh}$ B, PMS = 1.5 mm, HFZ = 150 mg L^{-1} , pH = 7, rt. b) Removal of different organic pollutants by HFZ/PMS system, reaction condition: $100 \text{ mL} 50 \text{ mg L}^{-1}$ organic pollutant, PMS = 1.5 mm, HFZ = 150 mg L^{-1} , pH = 7, rt.

The effect of different HFZ contents on Rh B degradation, while keeping the amounts of PMS and Rh B concentration the same, is shown in Figure 4c. The results show that a higher HFZ amount enhances the degradation of Rh B. With the catalyst amount rising from 50 to 200 mg L⁻¹, the Rh B removal efficiency improved accordingly. The pseudo-first-order reaction rate constant also confirms this conclusion. The reaction rate constants kunder different HFZ dosages were 0.456, 0.583, and 0.825 min⁻¹ (Figure \$7, Supporting Information), respectively. This is due to the enhanced availability of active sites in the reaction system, which facilitates PMS activation and produces more reactive oxygen species. However, compared with the catalyst content of 150 mg L⁻¹, the rate constant of 200 mg L⁻¹ only increased by 0.04 min⁻¹, and there was no significant improvement. This may be because the partially saturated active site in the 200 mg L⁻¹ catalyst is not used when the amount of PMS is limited. Considering the catalyst cost factors, the optimal catalyst dosage selected in this study is 150 mg L^{-1} .

The starting pH value is a crucial factor influencing the catalytic performance of the HFZ/PMS system. Therefore, its effect was evaluated at pH 3, 5, 7, 9, and 11 (Figure 4d). At pH = 7, the Rh B removal efficiency reaches its peak, achieving 100% removal within 10 min. At pH = 5, 97.6% of Rh B was removed within the same time. At pH values of 3 and 9, more than 94% of Rh B was removed within 10 min. When the pH is raised to 11, the removal efficiency drops significantly, with only 2% of Rh B removed in 1 min, 18.1% within 10 min, and 38.4% by 20 min. This trend is also reflected in the reaction rate constants. At pH values of 3, 5, 7, and 9, the degradation rate constant k is 0.529, 0.598, 0.825, and 0.448 min^{-1} , respectively. And when pH = 11, the reaction rate constant is only 0.0165 min⁻¹ (Figure S8, Supporting Information). This reduced efficiency at high alkalinity is likely due to PMS self-decomposing without producing SO4*-, thus lowering the degradation efficiency of Rh B.[22] It is clear that the HFZ/PMS system exhibits excellent catalytic activity across a broad pH range (3–9), with the highest efficiency at pH = 7.

Therefore, to further explore the application of the HFZ system in actual water bodies, we also conducted an experiment to evaluate the removal of Rh B by the HFZ/PMS system in river water taken from the Roter main river in Bayreuth, Germany, the pH value of the river water is 7.98 (Figure 5a). Compared with laboratory pure water, the removal process of Rh B in the

river water in the early stage of the reaction is relatively slow (52.8%). The removal efficiency increased to 99% when the reaction lasted for 10 min ($k = 0.437 \, \mathrm{min^{-1}}$) and completed degradation in $\approx 20 \, \mathrm{min}$ (Figure S9, Supporting Information). This demonstrates that HFZ can maintain high PMS activation performance in real water, indicating the potential for practical application of the HFZ/PMS system.

The system was also evaluated using four typical organic pollutants: methylene blue (MB), tetracycline (TC), bisphenol A (BPA), and Congo red (CR). Their chemical structures can be found in Figure \$10 (Supporting Information). The adsorption capacities of HOF for these pollutants were 314.7 mg g⁻¹ for MB, 365.1 mg g^{-1} for TC, 530.1 mg g^{-1} for BPA, and 111.1 mg g⁻¹ for CR. The observed enrichment is generally attributed to a combination of the material's porous structure and electrostatic interactions. Notably, the negatively charged CR showed the lowest adsorption, likely due to unfavorable electrostatic interactions. In the actual experiment, the removal efficiencies of MB, TC, BPA, and CR within 20 min using the HFZ/PMS system were 100%, 96.7%, 95.9%, and 98%, respectively (Figure 5b). This demonstrates that the HFZ/PMS system is effective for decomposing a variety of organic pollutants.

To better understand the reactive oxygen species generated during the reaction and the Rh B removal process, scavenger experiments were conducted. Methanol (MeOH) and tert-butanol (TBA) are well-known scavengers for SO4 - and OH radicals.[23] Furfuryl alcohol (FFA) is commonly used as a scavenger for nonfree radical ¹O₂, while sodium azide (NaN₂) helps identify ¹O₂, SO4° -, and OH.[24] The results, depicted in Figure 6a indicate that 1 M MeOH and TBA respectively inhibited Rh B degradation. Within 10 min, the efficiency of Rh B degradation declined to 87.1% and 94.6%, respectively. The result shows that PMS produced SO₄ • and OH, respectively, during the reaction process. However, the addition of TBA only slightly inhibited the removal of Rh B during the reaction, indicating that 'OH has no significant role in the reaction. With the addition of 10 mм FFA to the reaction system, the Rh B degradation efficiency dropped to 51.7% within 10 min which indicated that non-free radicals ¹O₂ were also produced. Also, with the addition of 10 mm NaN₃, Rh B could hardly be degraded. Those results confirm that the reactive oxidation species SO₄•-, OH, and ¹O₂ are generated, among

and-conditions) on Wiley Online Library for rules of use; OA articles are governed by the applicable Creative Commons

www.afm-journal.de

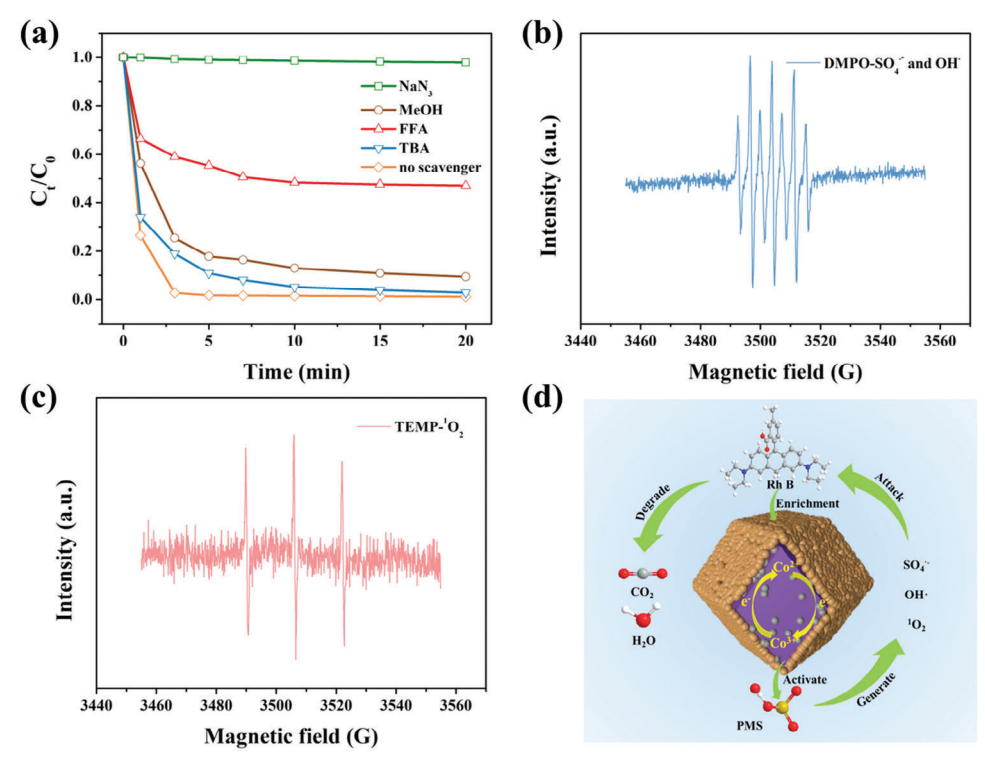


Figure 6. a) The removal of Rh B in different scavenger systems. EPR spectra of b) $^{\cdot}$ OH, SO₄ $^{\bullet}$ and c) 1 O₂ in Rh B solution. Reaction condition: 100 mL 50 mg L $^{-1}$ Rh B, PMS = 1.5 mm, HFZ = 150 mg L $^{-1}$, pH = 7, rt. d) Possible degradation mechanism of Rh B in HFZ/PMS system.

them, $SO_4^{\bullet -}$ and 1O_2 being the main contributors to Rh B degradation.

Electron paramagnetic resonance (EPR) experiments were used to further identify the reactive oxidation species that may form during the degradation process of Rh B, to prove the aforementioned result. $SO_4^{\bullet-}$, OH, and 1O_2 were captured using 5, 5-dimethyl-1-pyrroline (DMPO) and 2, 6, 6-tetramethyl-4-piperidone (TEMP). As shown in Figure 6b, when we used DMPO as the capture agent to verify the presence of SO₄•-, OH, we found that there is only one DMPOX (5,5-dimethyl-2oxo-pyrrolidine-1-oxy), the seven-element signal peak. But this does not mean that SO4 • - and OH are not produced during the reaction. This is attributed to the ultrafine splitting of DMPO oxidation products, indicating that DMPO may be strongly oxidized by SO4 •-, OH, and other strong oxidants during the reaction.[10,25] When TEMP was used as the capture agent for EPR experiments (Figure 6c), a triple signal peak was successfully detected, which was the characteristic peak of TEMP-1O₂. This result confirmed the generation of ¹O₂ during the reaction.^[26]

Combining the above experimental results, the possible degradation mechanism of Rh B removal by HFZ/PMS was proposed. The results are shown in Figure 6d. Rh B is adsorbed to the catalyst surface due to the porous structure and electrostatic interaction of the HOF shell, leading to the enrichment of Rh B molecules on the catalyst surface. This process effectively shortens the reaction pathway during the degradation process. $\rm Co^{2+}$ can activate $\rm HSO_5^-$ producing $\rm SO_4^{\bullet-}$ and $\rm ^{\circ}OH.^{[27]}$ The cobalt ions in the ZIF-67 core of HFZ can switch between $\rm Co^{2+}$ and $\rm ^{\circ}Co^{2+}$ states and $\rm ^{\circ}O_2$ is produced by the breaking of O—O bond in HSO₅-.[21b,28] Besides, during the entire reaction process, the

magnetic Fe_3O_4 as the electron donor in the HFZ supports the charge transfer and promotes the cycling between Co^{2+} and Co^{3+} , which on reaction with PMS generates SO_4^{\bullet} , thereby speeding up the removal rate of Rh B.

To evaluate the reusability of HFZ in PMS activation, five Rh B degradation cycles were performed (**Figure 7a**). After five cycles, the removal efficiency of Rh B can still reach 93.6%. More importantly, the XRD patterns show that the crystal structure of HFZ does not change significantly between the fresh and after use (Figure 7b). The above results demonstrated that HFZ, as a catalyst for activating PMS, exhibited high recyclability and good stability. Moreover, after 5 cycles of use, inductively coupled plasma optical emission spectrometry (ICP-OES) detected only 0.14 mg L⁻¹ cobalt ion leaching, which indicates that under the protection of the HOF shell, cobalt ion leaching problems can be effectively slowed down during use.

The possible degradation pathways of Rh B during the degradation process were analyzed using high-pressure liquid chromatography and mass spectroscopy (HPLC-MS), and the intermediates and their m/z values were identified (Figure S11, Supporting Information). According to the experimental results and previous reports, the degradation pathway of Rh B is mainly divided into four processes as shown in Figure S12 (Supporting Information). [29] First, N-de-ethylation generates m/z = 387, m/z = 359, and m/z = 331 intermediates, and then the chromophore structure is broken and degraded (m/z = 255, 213, 212). With the conjugated chromophore structure upon destruction, the reaction mixture becomes more complex, and a subsequent ring-opening process occurs, producing some primary oxidation products (m/z = 148, 99, 83), which are further degraded into

www.afm-journal.de

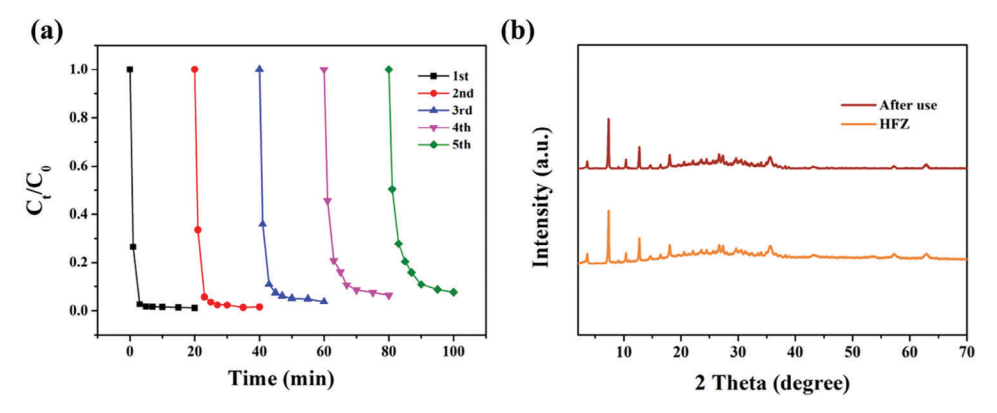


Figure 7. a) Reusability of HFZ activated PMS for degradation of Rh B. b) The XRD patterns of HFZ between the fresh and after use.

smaller compounds (m/z = 74). The subsequently formed oxidation intermediates are further mineralized into water, carbon dioxide, and other small molecule compounds of inorganic salt.

3. Conclusion

In this study, a magnetic HOF-on-MOF core-shell catalyst (HOFon-Fe₃O₄/ZIF-67) with ZIF-67 incorporating magnetic Fe₃O₄ as the core was successfully created and characterized for its morphology and crystal structure using SEM, TEM, XRD, and FT-IR. Under optimal conditions (Rh B = 50 mg L^{-1} , HFZ = 150 mg L^{-1} , $PMS = 1.5 \text{ mM}, pH = 7, room temperature}$, the HFZ/PMS system achieved complete Rh B degradation within 10 min, demonstrating high catalytic activity across a broad pH range (3-9). Under the protection of the HOF shell, the amount of cobalt ion leached out was negligible (0.14 mg L⁻¹ after 5 cycles). In addition, the catalyst shows satisfactory catalytic effect in different water quality and can degrade different types of organic pollutants, which provides a basis for its application in practice use. By scavenger experiments, EPR and HPLC-MS the reactive oxidation species produced during the reaction investigated and suggested a potential mechanism for Rhodamine degradation. In conclusion, this strategy offers new insights for developing core-shell MOF-HOF structure composite materials.

4. Experimental Section

Preparation of Fe_3O_4 Nanoparticles: The preparation of the particles was based on previously reported literature. In brief, 5 mmol of $FeSO_4 \cdot 7H_2O$ and 5 mmol of $FeCI_3 \cdot 6H_2O$ were mixed with 15 mL of Milli-Q water to form a clear orange solution which was then added dropwise to 20 mL of 3.5 mol L⁻¹ ammonia water at 60 °C. After ultrasound irradiation, the contents were reacted for 30 min, after which the black nanoparticles were separated and collected using a magnetic, repeatedly washed with water and methanol, and vacuum dried at 65 °C overnight.

Preparation of HOF: 100 mg 6,6′,6″,6″'-(Pyrene-1,3,6,8-tetrayl)tetrakis (2-naphthoic acid) (H_4 TNAPy) was dissolved in 30 mL of DMF under heating at 120 °C for 2 h to get a clear yellow solution [15]. Once cooled to room temperature, the solution was added to acetone (200 mL) and kept on stirring (\approx 270 rpm) for 12 h. Afterward, a yellow powder was isolated by centrifugation at 8500 rpm for 5 min. The obtained yellow powder was further washed with acetone (3 \times 30 mL) and then dried at ambient conditions.

Preparation of ZIF-67: In a typical process, $0.145 \text{ g Co}(NO_3)_2 \cdot 6H_2O$ and 2.37 g of 2-MeIM were each dissolved in 12 mL of water forming solutions A and B, respectively. Solution B was rapidly added to solution A at room temperature and stirred for 12 h, resulting in the formation of purple particles. These particles were separated by centrifugation, rinsed with water and methanol (3 \times 30 mL), and oven-dried at 80 °C to produce ZIF-67 particles.

Preparation of HOF-on-Fe₃O₄/ZIF-67 (HFZ): 115 mg of Fe₃O₄ was dispersed in water (16 mL) and named as solution A. Separately, 290 mg of Co(NO₃)₂·6H₂O and 4.7 g of 2-MeIm were dissolved in 16 mL of water to create solutions B and C, respectively. At room temperature, solution B was introduced into the solution A while stirring. After 1 h, solution C was introduced to the mixture, and stirring continued for an additional 12 h. The Fe₃O₄/ZIF-67 particles were then collected using a magnet for later use. Next, 100 mg of H₄TNAPy was dissolved in 30 mL of DMF and heated at 120 °C for 2 h to obtain a clear yellow solution. After cooling to room temperature, this solution was poured into 200 mL of a 500 mg L⁻¹ Fe₃O₄/ZIF-67 acetone dispersion within 3 min while stirring at 270 rpm. The suspension was stirred overnight. Finally, the HFZ particles were collected using the magnet, washed with acetone (5 \times 30 mL), and dried in a vacuum oven at 80 °C. The preparation of HOF-on-ZIF-67 is the same as HFZ except that there is no need to add solution A (Fe₃O₄), and solution B was added directly to solution C.

Adsorption Experiment: For the adsorption experiments, the adsorbent dosage, solution volume, temperature, and stirring speed were 10 mg, 20 mL, 25 °C, and 200 rpm, respectively. The amount of undegraded dye was measured by UV–vis spectroscopy at an absorption wavelength of $\lambda_{max}=555$ nm and using a standard calibration curve. The following Equation (1) was used:

$$q_e = (C_0 - C_e) \cdot V \cdot m^{-1} \tag{1}$$

where q_e (mg g⁻¹): equilibrium adsorption; C_0 (mg L⁻¹): initial concentration; C_e (mg L⁻¹): residual concentration at equilibrium; V (L): volume of Rh B solution used and m (g): mass of adsorbent used.

Catalytic Degradation Experiment: In a general reaction procedure, 100 mL, 50 mg L^{-1} of Rh B and PMS were added to the glass container, and then the reaction was activated by adding a catalyst (HFZ). At a desired time, 0.5 mL of the reaction solution was collected and immediately mixed with 0.5 mL of methanol to quench the reaction. A UV–vis spectrophotometer was used to determine the reaction concentrations. All experiments were conducted in triplicate.

Analytic Methods: The concentration of Rh B, MB, and TC in aqueous solution was measured by UV-vis spectrophotometer (Jasco Spectrometer V-670) at wavelength 555, 665, and 355 nm. The concentration of BPA in aqueous solution was measured by HPLC-MS, a UV wavelength of 230 nm. Rh B degradation intermediates were identified using high-pressure liquid chromatography-mass spectroscopy (HPLC-MS,

www.advancedsciencenews.com

www.afm-journal.de

VWR Chemicals, Germany), a welch ultimate C18 column (2.1×100 mm), a UV wavelength of 555 nm, mobile phase water (eluent A)/methanol (eluent B), gradient elution was listed as follows: 45% A/55% B (0–1.5 min), 25% A/75% B (1.5–14 min), 45% A/55% B (14–15 min), 45% A/55% B (15–25 min).

The degradation efficiency of pollutants was calculated according to Equation (2):

$$R\% = \frac{100\% \times (C_0 - C_t)}{C_0} \tag{2}$$

Which R is the degradation efficiency of pollutants (%), and C_0 is the concentration of pollutants at time 0, C_t is the concentration of pollutants at time t (mg L⁻¹).

And the kinetics of pollutants degradation process was investigated according to the pseudo first-order kinetics Equation (3):

$$-\ln\left(\frac{C_t}{C_0}\right) = kt\tag{3}$$

Where k is the degradation rate constant and t is the degradation time (min).

Supporting Information

Supporting Information is available from the Wiley Online Library or from the author.

Acknowledgements

Y.Du would like to thank the China Scholarship Council (CSC) for awarding a fellowship for carrying out Ph.D. research in Germany in the lab of Prof. Seema Agarwal. C. Deng thanks the Alexander von Humboldt Foundation for a postdoctoral fellowship and the financial support from the National Natural Science Foundation of China (22208162). S. Agarwal and S. Banerjee also acknowledge SPARC, Government of India for the support through a project (SPARC/2024-2025/ENSU/P3689).

Open access funding enabled and organized by Projekt DEAL.

Conflict of Interest

The authors declare no conflict of interest.

Data Availability Statement

The data that support the findings of this study are available in the supplementary material of this article.

Keywords

hydrogen-bonded organic framework, metal–organic frameworks, SR-AOP

Received: September 7, 2024 Revised: October 6, 2024 Published online:

a) Y. Yan, Z. Wei, X. Duan, M. Long, R. Spinney, D. D. Dionysiou, R. Xiao, P. J. J. Alvarez, *Environ. Sci. Technol.* 2023, *57*, 12153; b) J. Wang, S. Wang, *Chem. Eng. J.* 2020, *401*, 126158; c) H. S. Shahraki, R. Bushra, N. Shakeel, A. Ahmad, Quratulen, M. Ahmad, C. Ritzoulis, *J. Bioresour. Bioprod.* 2023, *8*, 162.

- [2] a) Y. Chen, H. Kang, M. Cheng, G. Zhang, G. Wang, H. Liu, W. Xiao, Y. Liu, H. Jiang, Adv. Funct. Mater. 2024, 34, 2309223; b) J. Lee, U. Von Gunten, J. H. Kim, Environ. Sci. Technol. 2020, 54, 3064.
- [3] a) C. Guo, M. Cheng, G. Zhang, W. Xiong, C. Zhou, B. Song, L. Du,
 L. Li, C. Tang, G. Wang, H. Liu, Environ. Sci.: Nano 2023, 10, 1528; b)
 J. Tan, X. Zhang, Y. Lu, X. Li, Y. Huang, Langmuir 2023, 40, 21.
- [4] X. Zheng, X. Niu, D. Zhang, M. Lv, X. Ye, J. Ma, Z. Lin, M. Fu, Chem. Eng. J. 2022, 429, 132323.
- [5] a) T. Yu, H. Chen, T. Hu, J. Feng, W. Xing, L. Tang, W. Tang, Appl. Catal. B 2024, 342, 123401; b) Y. Gao, T. Wu, C. Yang, C. Ma, Z. Zhao, Z. Wu, S. Cao, W. Geng, Y. Wang, Y. Yao, Y. Zhang, C. Cheng, Angew. Chem. Int. Ed. 2021, 60, 22513; c) S. An, G. Zhang, T. Wang, W. Zhang, K. Li, C. Song, J. T. Miller, S. Miao, J. Wang, X. Guo, ACS Nano 2018, 12, 9441; d) Z. Wang, E. Almatrafi, H. Wang, H. Qin, W. Wang, L. Du, S. Chen, G. Zeng, P. Xu, Angew. Chem., Int. Ed. 2022, 61, 202202338.
- [6] L. Chen, H. Ji, J. Qi, T. Huang, C. C. Wang, W. Liu, Chem. Eng. J. 2021, 406, 126877.
- [7] a) H. S. Jadhav, H. A. Bandal, S. Ramakrishna, H. Kim, Adv. Mater. 2022, 34, 2107072; b) R. Banerjee, A. Phan, B. Wang, C. Knobler, H. Furukawa, M. O'Keeffe, O. M. Yaghi, Science 2008, 319, 939; c) G. Zhong, D. Liu, J. Zhang, J. Mater. Chem. A 2018, 6, 1887; d) D. Saliba, M. Ammar, M. Rammal, M. Al-Ghoul, M. Hmadeh, J. Am. Chem. Soc. 2018, 140, 1812.
- [8] a) M. Kohantorabi, S. Giannakis, G. Moussavi, M. Bensimon, M. R. Gholami, C. Pulgarin, J. Hazard. Mater. 2021, 413, 125308; b) S. Ma, D. Yang, Y. Guan, Y. Yang, Y. Zhu, Y. Zhang, J. Wu, L. Sheng, L. Liu, T. Yao, Appl. Catal. B 2022, 316, 121594; c) C. Zhu, S. Zhao, Z. Fan, H. Wu, F. Liu, Z. Chen, A. Li, Adv. Funct. Mater. 2020, 30, 2003947.
- [9] Y. Li, J. Feng, Y. Zhang, C. Wang, J. Hao, Y. Wang, Y. Xu, X. Cheng, Chemosphere 2023, 311, 137038.
- [10] Z. Wu, Y. Wang, Z. Xiong, Z. Ao, S. Pu, G. Yao, B. Lai, Appl. Catal. B 2020, 277, 119136.
- [11] H. Wan, J. Yan, C. Guo, Q. Cui, W. Zhang, Environ. Res. 2022, 204, 111986.
- [12] a) R. B. Lin, Y. He, P. Li, H. Wang, W. Zhou, B. Chen, Chem. Soc. Rev. 2019, 48, 1362; b) R. B. Lin, B. Chen, Chem 2022, 8, 2114; c) I. Hisaki, C. Xin, K. Takahashi, T. Nakamura, Angew. Chem., Int. Ed. 2019, 12, 11160; d) C. A. Halliwell, S. E. Dann, J. Ferrando-Soria, F. Plasser, K. Yendall, E. V. Ramos-Fernandez, G. T. Vladisavljević, M. R. Elsegood, A. Fernandez, Angew. Chem. 2022, 134, 202208677.
- [13] a) X. Song, Y. Wang, C. Wang, D. Wang, G. Zhuang, K. O. Kirlikovali, P. Li, O. K. Farha, J. Am. Chem. Soc. 2022, 144, 10663; b) S. Goswami, K. Ma, J. Duan, K. O. Kirlikovali, J. Bai, J. T. Hupp, P. Li, O. K. Farha, Langmuir 2022, 38, 1533; c) B. Wang, R. B. Lin, Z. Zhang, S. Xiang, B. Chen, J. Am. Chem. Soc. 2020, 142, 14399.
- [14] R. Wagia, I. Strashnov, M. W. Anderson, M. P. Attfield, Cryst. Growth Des. 2018, 18, 695.
- [15] K. Ma, P. Li, J. H. Xin, Y. Chen, Z. Chen, S. Goswami, X. Liu, S. Kato, H. Chen, X. Zhang, J. Bai, M. C. Wasson, R. R. Maldonado, R. Q. Snurr, O. K. Farha, Cell Rep. Phys. Sci. 2020, 1, 100024.
- [16] Y. Du, C. Ding, S. Agarwal, Adv. Energy Sustainability Res. 2024, 5, 2300218.
- [17] Z. Dong, Q. Zhang, B. Y. Chen, J. Hong, Chem. Eng. J. 2019, 357, 337.
- [18] Y. Wei, Y. Han, X. Hu, Y. Lin, X. Wang, X. Deng, Procedia Eng. 2012, 27, 632.
- [19] a) Q. Yang, S. Ren, Q. Zhao, R. Lu, C. Hang, Z. Chen, H. Zheng, Chem. Eng. J. 2018, 333, 49; b) Z. Li, G. Zhou, H. Dai, M. Yang, Y. Fu, Y. Ying, Y. Li, J. Mater. Chem. A 2018, 6, 3402.
- [20] Y. Guo, C. Zhou, X. Lv, S. Du, M. Sui, Sep. Purif. Technol. 2024, 35, 128729.
- [21] a) X. Zhang, J. Zhang, B. Hou, X. Yang, J. Ren, C. Shao, Appl. Surf. Sci. 2024, 643, 158663; b) X. Wu, D. Sun, H. Ma, C. Ma, X. Zhang, J. Hao, Colloids Surf., A 2022, 637, 128278; c) J. Cui, T. Liu, Q. Zhang, T. Wang, X. Hou, Chem. Eng. J. 2021, 404, 126453;

www.advancedsciencenews.com



www.afm-journal.de

- d) S. Lu, S. You, J. Hu, X. Li, L. Li, *RSC adv.* **2024**, *14*, 7528; e) L. Peng, X. Gong, X. Wang, Z. Yang, Y. Liu, *RSC Adv.* **2018**, *8*, 26377; f) Y. Li, X. Yan, X. Hu, R. Feng, M. Zhou, *Chem. Eng. J.* **2019**, *375*, 122003.
- [22] a) F. Wang, H. Fu, F. X. Wang, X. W. Zhang, P. Wang, C. Zhao, C. C. Wang, J. Hazard. Mater. 2022, 423, 126998; b) D. L. Ball, J. O. Edwards, J. Am. Chem. Soc. 1956, 78, 1125.
- [23] a) T. B. Nguyen, V. A. Thai, C. W. Chen, C. P. Huang, R. A. Doong, L. Chen, C. D. Dong, Sep. Purif. Technol. 2022, 288, 120719; b) Y. Xu, J. Ai, H. Zhang, J. Hazard. Mater. 2016, 309, 87
- [24] a) Z. Weng, Y. Lin, S. Guo, X. Zhang, Q. Guo, Y. Luo, X. Ou, J. Ma, Y. Zhou, J. Jiang, B. Han, Angew. Chem. 2023, 135, 2023 10934; b) Y. Li, J. Li, Y. Pan, Z. Xiong, G. Yao, R. Xie, B. Lai, Chem. Eng. J. 2020, 384,

- 123361; c) M. Ahmadi, F. Ghanbari, Environ. Sci. Pollut. Res. 2018, 25, 6003.
- [25] W. Ma, N. Wang, T. Tong, L. Zhang, K. Y. A. Lin, X. Han, Y. Du, Carbon 2018, 137, 291.
- [26] Y. Zeng, J. Deng, N. Zhou, W. Xia, Z. Wang, B. Song, Z. Wang, Y. Yang, X. Xu, G. Zeng, C. Zhou, Small 2024, 20, 2311552.
- [27] C. Wang, P. Cheng, Y. Yao, Y. Yamauchi, X. Yan, J. Li, J. Na, J. Hazard. Mater. 2020, 392, 122164.
- [28] W. Zheng, Y. Sun, Y. Gu, Chem. Eng. J. 2023, 459, 141668.
- [29] a) Z. He, C. Sun, S. Yang, Y. Ding, H. He, Z. Wang, J. Hazard. Mater. 2009, 162, 1477; b) Q. Zhong, J. Liu, J. Wang, Y. Li, J. Li, G. Zhang, Chemosphere 2022, 300, 134564.
- [30] M. Chen, N. Wang, X. Wang, Y. Zhou, L. Zhu, Chem. Eng. J. 2021, 413, 127539.